



Effects of lithium excess amount on the microstructure and electrochemical properties of $\text{LiNi}_{0.5}\text{Mn}_{1.5}\text{O}_4$ cathode material

Jianling Guo^{1,2,3} · Xing Qin^{1,2,3} · Bo Zong^{1,2,3} · Mushang Zhou^{1,2,3} · Wei Wu^{1,2,3} · Li Wang^{1,2,3}

Received: 9 September 2017 / Revised: 24 November 2017 / Accepted: 28 November 2017 / Published online: 9 December 2017
© Springer-Verlag GmbH Germany, part of Springer Nature 2017

Abstract

Spinel $\text{LiNi}_{0.5}\text{Mn}_{1.5}\text{O}_4$ cathode materials with different lithium excess amount (0, 2%, 6%, 10%) were synthesized by a facile solid-state method. The effect of lithium excess amount on the microstructure, morphology, and electrochemical properties of $\text{LiNi}_{0.5}\text{Mn}_{1.5}\text{O}_4$ materials was systematically investigated. The results show that the lithium excess amount does not change the particle morphology and size obviously; thus, the electrochemical properties of $\text{LiNi}_{0.5}\text{Mn}_{1.5}\text{O}_4$ are mainly determined by structural characteristics. With the increase of lithium excess amount, the cation disordering degree (Mn^{3+} content) and phase purity first increase and then decrease, while the cation mixing extent has the opposite trend. Among them, the $\text{LiNi}_{0.5}\text{Mn}_{1.5}\text{O}_4$ material with 6% lithium excess amount exhibits higher disordering degree and lower impurity content and cation mixing extent, thus leading to the optimum electrochemical properties, with discharge capacities of 125.0, 126.1, 124.2, and 118.9 mAh/g at 0.2-, 1-, 5-, and 10-C rates and capacity retention rate of 96.49% after 100 cycles at 1-C rate.

Keywords Lithium-ion battery · Cathode material · $\text{LiNi}_{0.5}\text{Mn}_{1.5}\text{O}_4$ · Lithium excess amount · Electrochemical performance

Introduction

Lithium ion batteries have been regarded as one of the most promising power sources and energy storage devices due to long cycle life, high energy density, and environmental friendliness [1–3]. Nevertheless, the battery with high energy and power density is emergently required to meet the needs for electric vehicles (EVs) and hybrid-electric vehicles (HEVs) [4]. It is well known that the energy density is mainly determined by the cathode material, which can be achieved by improving the working potential and discharge capacity

because the energy density is the product of voltage and discharge capacity. Among the cathode materials, $\text{LiNi}_{0.5}\text{Mn}_{1.5}\text{O}_4$ spinel has received significant interest because it can offer a high operating voltage of ~ 4.7 V (vs. Li/Li^+) arising from $\text{Ni}^{2+}/\text{Ni}^{4+}$ redox couple and fast 3D lithium-ion diffusion channels within the cubic lattice [5–7]. Based on the high working voltage, $\text{LiNi}_{0.5}\text{Mn}_{1.5}\text{O}_4$ electrode can deliver an energy density of 650 Wh/kg, higher than that of LiCoO_2 (518 Wh/kg), LiMn_2O_4 (400 Wh/kg), LiFePO_4 (495 Wh/kg), and $\text{LiCo}_{1/3}\text{Ni}_{1/3}\text{Mn}_{1/3}\text{O}_2$ (576 Wh/kg) [7].

Depending on the distribution of Ni/Mn in octahedral $16d$ sites, $\text{LiNi}_{0.5}\text{Mn}_{1.5}\text{O}_4$ generally has two different crystallographic structures: the disordered $Fd3m$ space group with a random distribution of Mn/Ni ions in $16d$ sites and the ordered $P4_332$ space group with the ordered arrangement of Mn/Ni ions in $16d$ sites. Generally, there always exist some amounts of Mn^{3+} ions in $Fd3m$ space group, while only Mn^{4+} ions present in $P4_332$ space group. The presence and amount of Mn^{3+} ions are believed to have two opposite effects. On one hand, it can enhance the lithium-ion and electronic conductivity, which is conducive to rate capability [5]. On the other hand, Mn^{3+} ions are unstable and tend to undergo a disproportionation reaction: $2\text{Mn}^{3+} = \text{Mn}^{2+} + \text{Mn}^{4+}$, and the generated Mn^{2+} ions may dissolve into the electrolyte, thus leading to the capacity fading during charge/discharge cycling [8, 9].

Electronic supplementary material The online version of this article (<https://doi.org/10.1007/s11581-017-2374-5>) contains supplementary material, which is available to authorized users.

✉ Li Wang
wangli_hebut@163.com

¹ Institute of Power Source and Ecomaterials Science, Hebei University of Technology, Tianjin 300130, China

² Key Laboratory of Special Functional Materials for Ecological Environment and Information (Hebei University of Technology), Ministry of Education, Tianjin 300130, China

³ Key Laboratory for New Type of Functional Materials in Hebei Province, Hebei University of Technology, Tianjin 300130, China

Therefore, the Mn^{3+} content in $\text{LiNi}_{0.5}\text{Mn}_{1.5}\text{O}_4$ spinel should be optimized to achieve better overall electrochemical performance. Generally, the oxygen loss occurring at high-temperature calcination will obviously lead to the appearance of Mn^{3+} in the spinel. Besides, the Mn^{3+} content is affected by a cation doping [10, 11]. If the synthesis method is fixed, for instance, solid-state method, the Mn^{3+} content can be regulated by synthesis conditions (including the types and amounts of raw materials, calcination temperature and time, etc.), which have critical significance on the crystalline structure, then on the electrochemical performance.

Due to the lithium loss during high-temperature calcination process, the lithium amount is often in excess of the stoichiometric amount. However, to the best of our knowledge, there have been different conclusions about the effect of lithium excess amounts on the crystalline and electrochemical properties. Chen et al. [12] used porous MnCO_3 microsphere as precursor, and the lithium excess amount was chosen at 0, 2, 5, and 8%, respectively. They found that the $\text{Li}_x\text{Ni}_{1-x}\text{O}$ impurity phase is gradually increased with lithium excess amount increasing. The lattice parameter and Mn^{3+} content first increase and then decrease with the lithium excess amount, and the sample with 5% lithium excess amount has the largest lattice parameter and Mn^{3+} content. However, Deng et al. [13] synthesized octahedral $\text{LiNi}_{0.5}\text{Mn}_{1.5}\text{O}_4$ cathode materials through a one-step nonaqueous co-precipitation method, and the lithium excess amount was chosen at 0, 1, 3, and 5%. The XRD analysis indicated that increasing Li amount changed the structure from disordered to ordered phase and reduced the $\text{Li}_x\text{Ni}_{1-x}\text{O}$ impurity phase amount. Among them, the sample with 5% lithium excess amount has the smallest lattice parameter and Mn^{3+} content, which is just contrary to the results of Ref. [12]. We do not know whether the different results may be caused by the different synthesis methods or other reasons. In this paper, $\text{LiNi}_{0.5}\text{Mn}_{1.5}\text{O}_4$ cathode material was synthesized by a facile solid-state method, and the effects of different lithium excess amounts (0, 2, 6, and 10%) on the physicochemical properties as well as electrochemical properties were systematically investigated. The relationship between crystalline structure and electrochemical performance was extensively discussed.

Materials and methods

Sample synthesis

$\text{LiNi}_{0.5}\text{Mn}_{1.5}\text{O}_4$ samples with different lithium excess amounts were prepared by a facile solid-state method. The preparation process is just as follows. Stoichiometric amounts of Li_2CO_3 , NiO and Mn_3O_4 (corresponding to 0.2-mol $\text{LiNi}_{0.5}\text{Mn}_{1.5}\text{O}_4$) were mixed by ball milling for 1 h on a planetary ball miller at a rotation speed of 400 rpm and a ball-to-powder ratio of 20:1, then calcinated at 850 °C for

8 h at a heating rate of 5 °C/min in air atmosphere, and finally cooled naturally to room temperature to obtain the product. The involved chemical reaction is just as follows: $\text{Li}_2\text{CO}_3 + \text{NiO} + \text{Mn}_3\text{O}_4 + \text{O}_2 = 2\text{LiNi}_{0.5}\text{Mn}_{1.5}\text{O}_4 + \text{CO}_2$. The lithium excess amount was set as 0, 2, 6, and 10% (in weight), respectively, and the corresponding product was labeled as LNMO-0, LNMO-2%, LNMO-6%, and LNMO-10%, respectively.

Sample characterization

The crystalline phase of the synthesized samples was identified by X-ray diffraction (XRD) on a Bruker D8-FOCUS X-ray diffractometer using $\text{Cu K}\alpha$ ($\lambda = 0.15406$ nm) over 2θ range of 10–80°. Lattice parameters of the samples were calculated through structural refinements using Rietveld software. The particle morphology and size of the samples were determined by scanning electron microscopy (SEM) on a FEI Nova Nano SEM450 instrument. The discrimination of ordered and disordered structure of the samples was achieved by Fourier transformation infrared (FT-IR) on a Bruker V80 Fourier transformation infrared spectrometer over the range of 400–700 cm^{-1} .

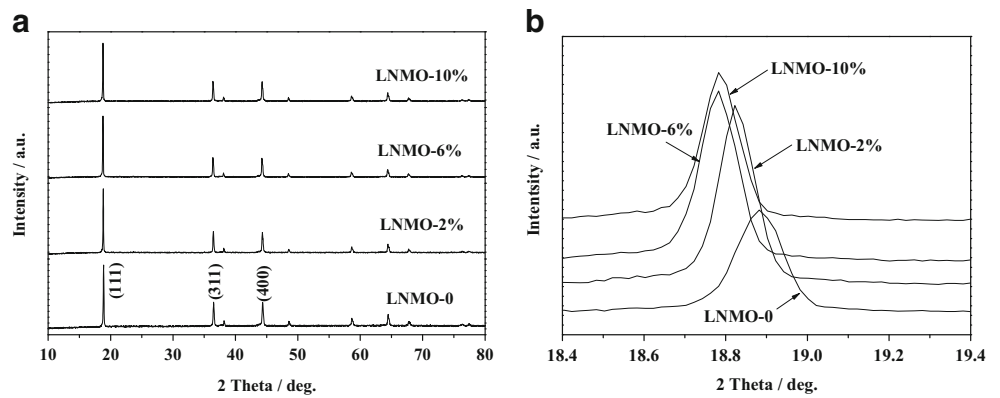
Electrochemical test

Electrochemical performance of the samples was measured using the CR-2032-type coin cell. The cathode was prepared as follows: 80 wt.% of synthesized powder, 15 wt.% ethylene black, and 5 wt.% PTFE were mixed in alcohol and then ultrasonically dispersed uniformly to form a slurry. After the evaporation of alcohol, the mixture was rolled to a thin film with a thickness of 0.14 mm. The round electrode plate with a diameter of 10 mm was cut down for coin assembly. The cells were assembled in an argon-filled glove box using lithium foil as the anode, Celgard 2400 as the separator, and 1-M LiPF_6 in EC:DMC:EMC (1:1:1 in volume) as the electrolyte. The cell was charged and discharged galvanostatically in a voltage range of 3.5–4.95 V (vs. Li/Li^+) at room temperature with different current densities. The electrochemical impedance spectroscopy (EIS) was measured using an electrochemical workstation (CHI660D) with an ac amplitude of 5 mV in a frequency range from 100 kHz to 10 mHz at fully discharged state after 3 cycles. The CV curves were also measured on CHI660D from 3.4 to 5.0 V at a scan rate of 0.1 mV/s.

Results and discussion

Figure 1a shows the XRD patterns of $\text{LiNi}_{0.5}\text{Mn}_{1.5}\text{O}_4$ materials with different lithium excess amounts. All four patterns can be assigned to a cubic spinel $\text{LiNi}_{0.5}\text{Mn}_{1.5}\text{O}_4$ with $Fd\bar{3}m$ space group (JCPDS Card No.: 80-2162). Besides, there exist some weak peaks at $2\theta = 37.5^\circ$, 43.6° , and 63.4° , which can

Fig. 1 XRD patterns (a) and magnified image of (111) peak (b) for $\text{LiNi}_{0.5}\text{Mn}_{1.5}\text{O}_4$ samples with different lithium excess amounts



be assigned to the rock-salt $\text{Li}_x\text{Ni}_{1-x}\text{O}$ impurity phase, due to the oxygen loss during calcination process. The content of impurity phase is estimated by calculating the ratio of peak intensity at $2\theta = 43.6^\circ$ of impurity phase to that at $2\theta = 44.3^\circ$ of spinel phase [14]. The intensity ratios in LNMO-0, LNMO-2%, LNMO-6%, and LNMO-10% samples are 14.4:100, 13.9:100, 9.4:100, and 10.9:100, respectively. The impurity content decreases in the order of LNMO-0 > LNMO-2% > LNMO-10% > LNMO-6%, and the sample LNMO-6% has the lowest impurity content. It is speculated that both the occupation of tetrahedral 8a site by nickel ions at lower lithium excess amount (0, 2%) and the occupation of octahedral 16d site by lithium ions at higher lithium excess amount (10%) force nickel ions out of their own octahedral 16d site, thus leading to the increase of impurity content.

Table 1 lists the lattice parameters of four samples obtained from the Rietveld refinement results based on $Fd3m$ space group. From the refinement factors listed in Table S1, it can be clearly seen that the refinement yields good agreement factors, with R_{wp} values less than 10% and GOF values between 1 and 2, suggesting an acceptable refinement. It can be seen that the lattice parameter a is 8.1787, 8.1796, 8.1800, 8.1774 Å, respectively, for LNMO-0, LNMO-2%, LNMO-6%, and LNMO-10% samples, that is, the lattice parameters first increase and then decrease with the lithium excess amount increasing, and the sample LNMO-6% shows the largest lattice parameter, which is believed to be advantageous to the lithium-ion diffusion, then to the electrochemical performance. From the magnified image of (111) diffraction peak in Fig. 1b, we can see that with the increase of lithium excess amount, the (111) diffraction peak shifts first toward lower angles and then slightly toward higher angles, which is in accordance with the variation of lattice parameter based on the Bragg equation $2d\sin\theta = n\lambda$. The variation of lattice parameter can be explained by Mn^{3+} content due to the larger ionic radius of Mn^{3+} ion (0.645 Å) than that of Mn^{4+} ion (0.53 Å). When lithium excess amount is increased from 0 to 6%, the excess Li^+ ions occupy the vacant tetrahedral 8a site caused by the lithium loss during high-temperature

calcination, which makes part of Mn^{4+} reduced to Mn^{3+} in order to maintain charge neutrality, thus leading to the initial increase of lattice parameter. However, when lithium excess amount is further increased to 10%, the lattice parameter is decreased on the contrary. This may be due to that there is no vacant tetrahedral 8a site, which forces the superfluous Li^+ ions to occupy the octahedral 16d site due to the similar ionic radius of Li^+ and Ni^{2+} ions, which is called “cation mixing.” This will make part of Mn^{3+} oxidized back to Mn^{4+} , thus leading to the decrease of lattice parameter at higher lithium excess amount of 10%.

In spinel structure, (111) diffraction peak is the strongest line, while in anti-spinel structure, (311) diffraction peak becomes the strongest line with location switching of A/B atoms in AB_2O_4 formula. Therefore, the I_{111}/I_{311} intensity ratio is an important implication for the cation mixing extent between Li^+ ions and transition metal ions in $\text{LiNi}_{0.5}\text{Mn}_{1.5}\text{O}_4$ spinel [15]. The higher the I_{111}/I_{311} intensity ratio, the lower the cation mixing extent between Li^+ ions and transition metal ions. Table 1 lists the I_{111}/I_{311} intensity ratios of four samples, which are 2.23, 2.65, 2.73, and 2.55 for LNMO-0, LNMO-2%, LNMO-6%, LNMO-10% samples, respectively, among which, the sample LNMO-6% has the highest I_{111}/I_{311} intensity ratio, suggesting its lowest cation mixing extent between Li^+ ions and transition metal ions. The lower cation mixing extent results in the smooth path for lithium transport; therefore, advanced rate capability is highly expected. At lower lithium excess amounts of 0 and 2%, the higher cation mixing extent may be ascribed to the occupation of vacant tetrahedral

Table 1 Lattice parameters, I_{111}/I_{311} and I_{311}/I_{400} ratios of $\text{LiNi}_{0.5}\text{Mn}_{1.5}\text{O}_4$ samples with different lithium excess amounts

Sample	a (Å)	V (Å ³)	I_{111}/I_{311}	I_{311}/I_{400}
LNMO-0	8.1787	547.08	2.23	0.998
LNMO-2%	8.1796	547.26	2.65	1.044
LNMO-6%	8.1800	547.35	2.73	1.049
LNMO-10%	8.1774	546.83	2.55	1.032

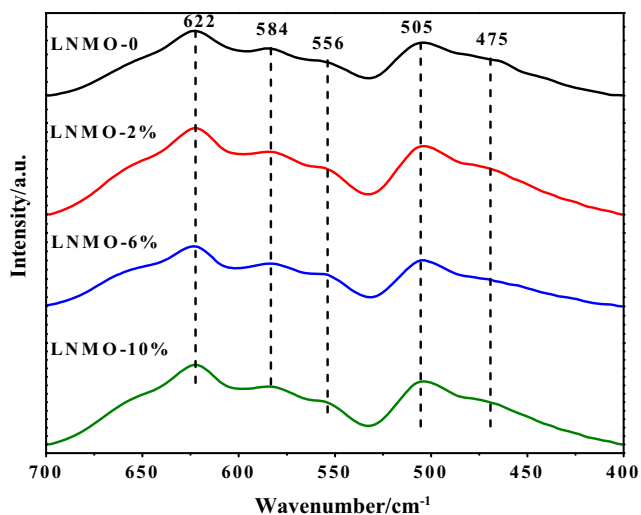


Fig. 2 FT-IR spectra of $\text{LiNi}_{0.5}\text{Mn}_{1.5}\text{O}_4$ samples with different lithium excess amounts

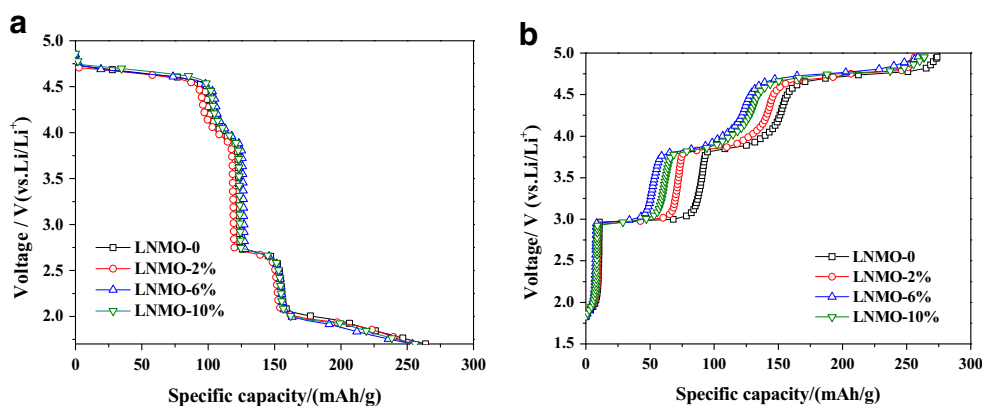
$8a$ sites by transition metal ions due to the lithium loss during high-temperature calcination. However, when lithium excess amount is as high as 10%, the I_{111}/I_{311} intensity ratio is decreased contrarily, implying a heavier cation mixing extent, which may be attributed to the occupation of octahedral $16d$ sites by superfluous Li^+ ions. The higher cation mixing extent is unfavorable to the structural stability, then to the cycling performance, as seen in Fig. 6.

It has been reported that the I_{311}/I_{400} peak intensity ratio can reflect the structural stability of the $[\text{Mn}_2]\text{O}_4$ spinel framework [16, 17]. Previous reports [18, 19] show that the spinel LiMn_2O_4 with the I_{311}/I_{400} intensity ratios between 0.96 and 1.1 usually shows better electrochemical performances than those outside this region. The higher I_{311}/I_{400} intensity ratio means better structural stability [20]. As shown in Table 1, the I_{311}/I_{400} intensity ratios of LNMO-0, LNMO-2%, LNMO-6%, and LNMO-10% are 0.998, 1.044, 1.049, and 1.032, respectively, all between 0.96 and 1.1. It is therefore reasonable to infer that all four $\text{LiNi}_{0.5}\text{Mn}_{1.5}\text{O}_4$ samples should possess good structural stability, among which, the LNMO-6%

sample exhibits the best structural stability, which can be manifested by the following cycling performance curves in Fig. 6. In addition, it has been reported that the difference of I_{311}/I_{400} intensity ratio may have something to do with the Mn^{3+} [15]. The higher Mn^{3+} content, the higher I_{311}/I_{400} intensity ratio, in consistence with our findings.

Due to the similar scattering factors of Ni and Mn, it is difficult to use XRD to distinguish ordered/disordered structure. FT-IR spectroscopy has been proven to be an effective technique to differentiate the ordered and disordered structures of the nickel-manganese spinel [21]. Figure 2 shows the FT-IR spectra of $\text{LiNi}_{0.5}\text{Mn}_{1.5}\text{O}_4$ samples with different lithium excess amounts. It is generally accepted that the ordered $P4_332$ phase exhibits eight well-defined absorption bands, while the disordered $Fd3m$ phase gives a rather broad spectrum with only five absorption bands [12, 22]. As shown in Fig. 2, all four spectra show only five bands, indicating the disordered structure of samples with different lithium excess amounts, in consistence with the XRD result. It has been reported that the $I(584\text{ cm}^{-1})/I(622\text{ cm}^{-1})$ intensity ratio can be used to qualitatively access the disordering degree, and the higher the intensity ratio, the lower the disordering degree of Ni/Mn at octahedral $16d$ site [22]. From Fig. 2, we can get that the $I(584\text{ cm}^{-1})/I(622\text{ cm}^{-1})$ intensity ratios are 0.7586, 0.7282, 0.7104, and 0.7267, respectively, for LNMO-0, LNMO-2%, LNMO-6%, and LNMO-10% samples, which indicates that the disordering degree first increases and then decreases with the lithium excess amount increasing, among which, the $\text{LiNi}_{0.5}\text{Mn}_{1.5}\text{O}_4$ sample with 6% lithium excess amount exhibits the highest disordering degree, in consistence with the variation of Mn^{3+} content in the spinel. The initial increase of disordering degree at lithium excess amount of 0 to 6% is due to that the superfluous Li^+ ions can compensate for the lithium loss during high-temperature calcination process and occupy the vacant tetrahedral $8a$ site, which leads to the reduction of Mn^{4+} to Mn^{3+} in order to maintain charge neutrality. However, when the lithium excess amount is further increased to 10%, the redundant Li^+

Fig. 3 First discharge curves (a) and second charge curves (b) of $\text{LiNi}_{0.5}\text{Mn}_{1.5}\text{O}_4$ samples with different lithium excess amounts



ions may occupy the octahedral $16d$ site, which makes part of Mn^{3+} oxidized back to Mn^{4+} , thus leading to the decrease of disordering degree of LNMO-10% in comparison with LNMO-6%. Therefore, it can be supposed that the lithium amount can adjust the phase structure, or rather, the disordering degree of $LiNi_{0.5}Mn_{1.5}O_4$ material, in consistence with the findings of Ref. [12].

In addition to the FT-IR bands normally used to assess the cation ordering, it has been reported that an examination of the charge/discharge behavior below 3 V involving the insertion/extraction of Li^+ ions into/from the empty $16c$ sites is an effective

way to assess the cation ordering degree in the 5-V spinels [23, 24]. Figure 3 illustrates the first discharge and second charge curves of $LiNi_{0.5}Mn_{1.5}O_4$ samples with different lithium excess amounts at 0.2-C rate in the voltage range of 1.7–5.0 V. It has been reported that longer ~ 2.7 -V plateau and shorter ~ 2.1 -V plateau in the first discharge curve mean higher disordering degree. As for the second charge curves, the longer ~ 3.8 -V plateau also means higher disordering degree [23, 24]. From Fig. 3, it can be seen that the disordering degree first increases and then decreases with the lithium excess amount increasing, and the $LiNi_{0.5}Mn_{1.5}O_4$ sample with 6% lithium excess amount exhibits

Fig. 4 SEM images of $LiNi_{0.5}Mn_{1.5}O_4$ samples with different lithium excess amounts. **a, b** LNMO-0. **c, d** LNMO-2%. **e, f** LNMO-6%. **g, h** LNMO-10%

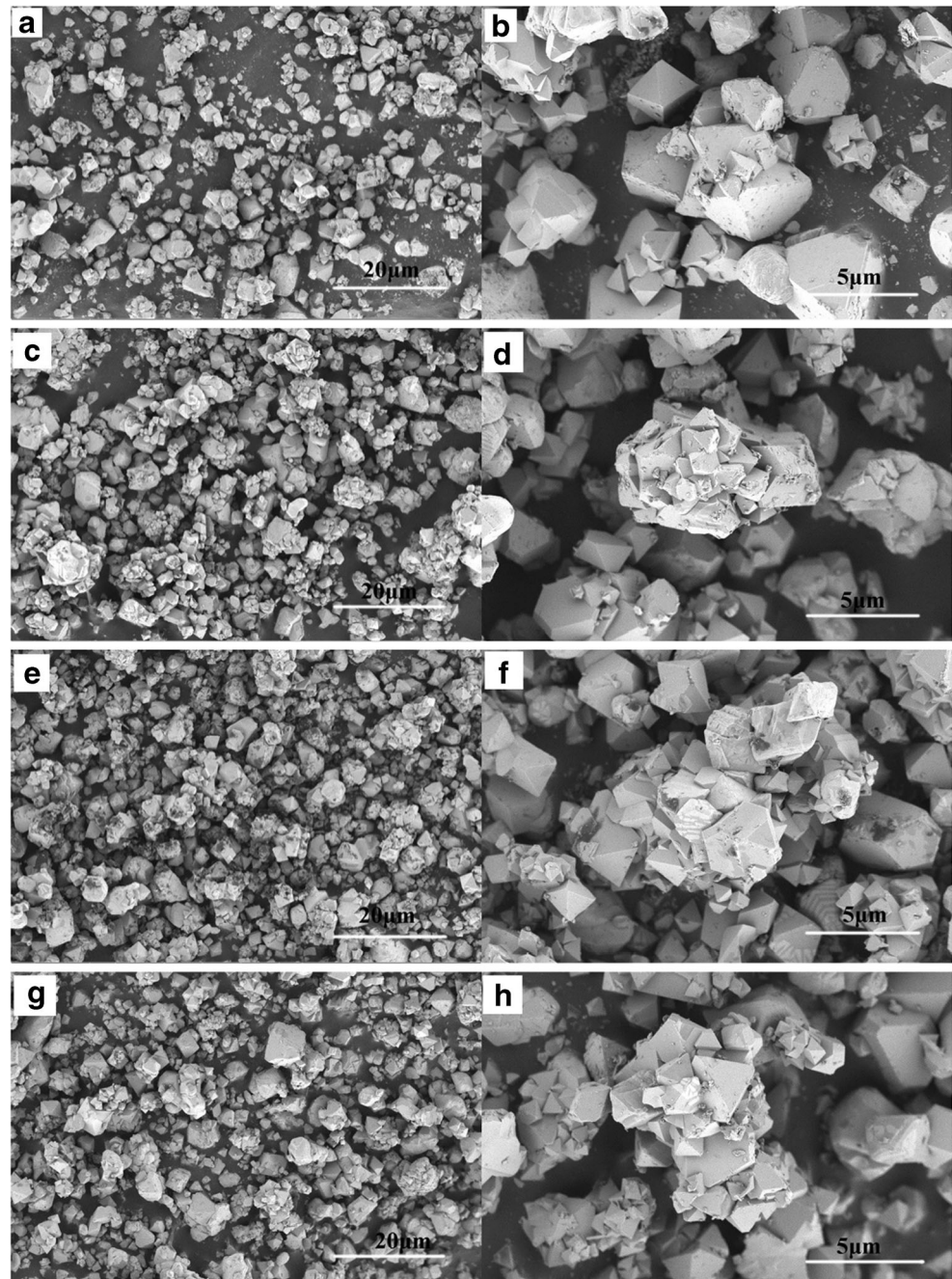
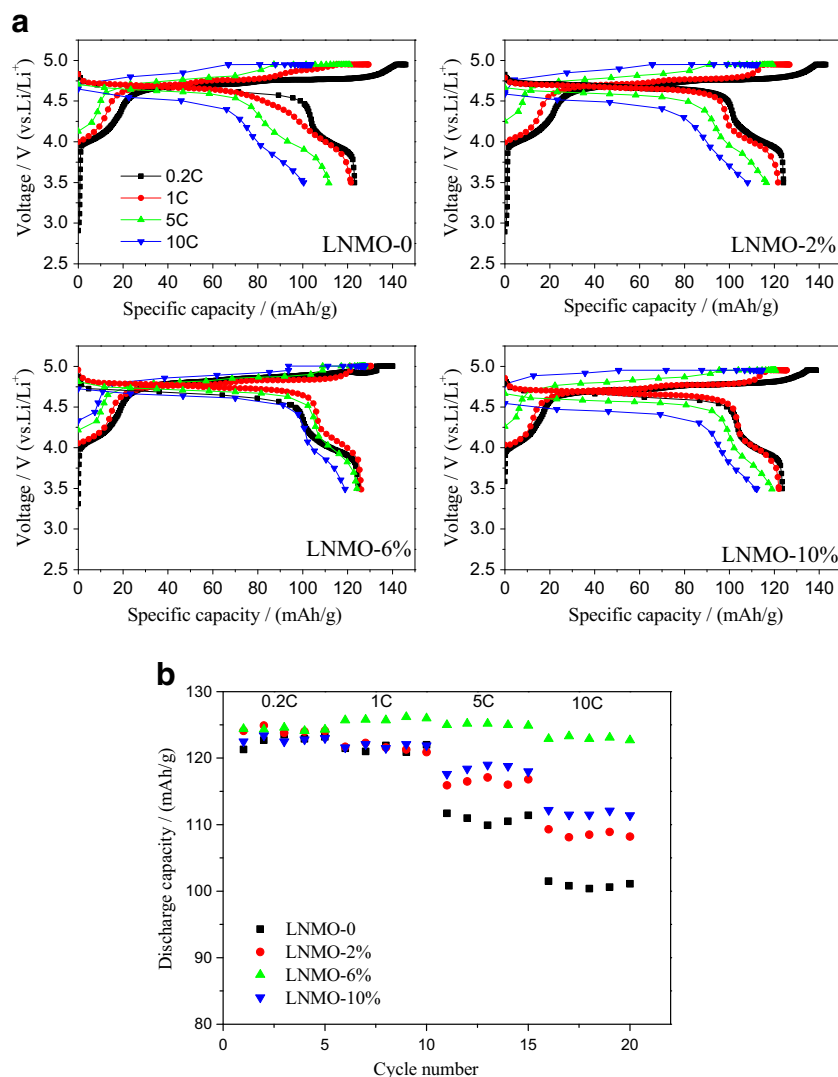


Fig. 5 Charge/discharge curves at various rates (a) and rate performance curves (b) for $\text{LiNi}_{0.5}\text{Mn}_{1.5}\text{O}_4$ samples with different lithium excess amounts



the highest disordering degree, in accordance with the FT-IR results, which indicates that appropriate lithium excess amount is favorable to the enhancement of disordering degree, then to the electrochemical properties.

Figure 4 shows the SEM images of $\text{LiNi}_{0.5}\text{Mn}_{1.5}\text{O}_4$ samples with different lithium excess amounts. From Fig. 4, we can see that all samples show similar morphology, that is, the secondary aggregates composed of octahedral primary particles with clean surface. Therefore, the influence of particle morphology on the electrochemical performance can be excluded, and the relationship between crystal structure and electrochemical performance of $\text{LiNi}_{0.5}\text{Mn}_{1.5}\text{O}_4$ samples can be better understood.

Figure 5a shows the charge/discharge curves of $\text{LiNi}_{0.5}\text{Mn}_{1.5}\text{O}_4$ samples with different lithium excess amounts at 0.2-, 1-, 5-, and 10-C rates. From the discharge curves at 0.2-C rate, it can be seen that all samples have a major discharge plateau at ~ 4.7 V and a minor discharge plateau at ~ 4.0 V, which can be assigned to $\text{Ni}^{2+}/\text{Ni}^{4+}$ and $\text{Mn}^{3+}/$

Mn^{4+} redox couples, respectively. The existence of ~ 4.0 -V plateau implies the existence of Mn^{3+} ions in spinel structure, whose content can be calculated by the discharge capacity between 3.80 and 4.25 V divided by the total discharge

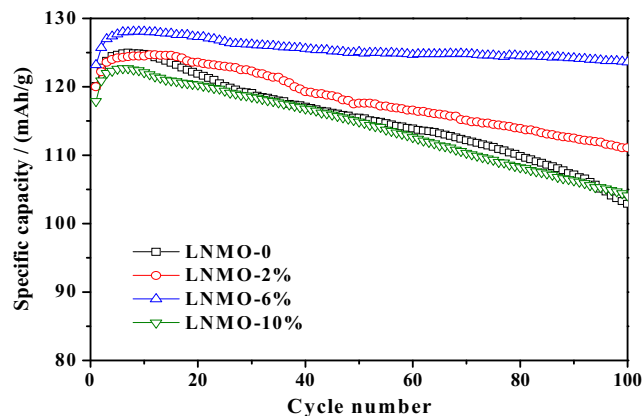
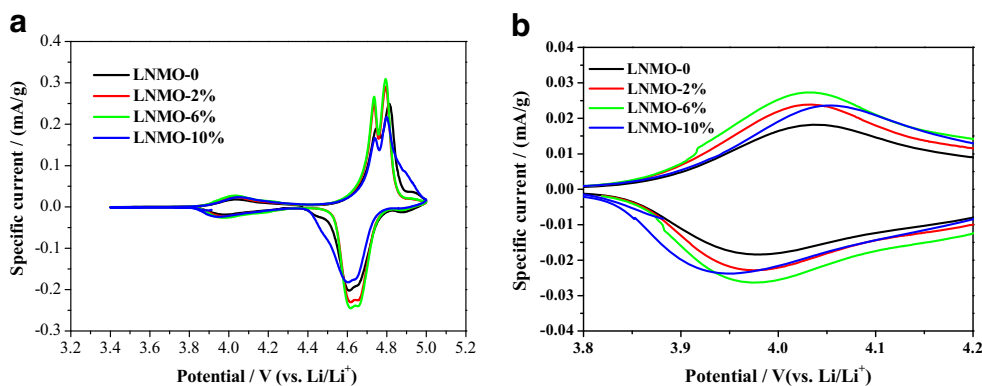


Fig. 6 Cycling performance curves of $\text{LiNi}_{0.5}\text{Mn}_{1.5}\text{O}_4$ samples with different lithium excess amounts at 1-C rate

Fig. 7 CV curves (a) and the magnification image of ~4.0-V peak (b) of $\text{LiNi}_{0.5}\text{Mn}_{1.5}\text{O}_4$ samples with different lithium excess amounts



capacity at 0.2-C rate [25]. The relative Mn^{3+} contents are 14.62, 16.60, 17.68, and 15.13%, respectively, for LNMO-0, LNMO-2%, LNMO-6%, LNMO-10% samples. It can be seen that the Mn^{3+} content (disordering degree) first increases and then decreases with the lithium excess amount, consistent with the results of Figs. 1, 2, and 3.

From Fig. 5a, we know that the 0.2-C discharge capacities of LNMO-0, LNMO-2%, LNMO-6%, and LNMO-10% samples are 123.1, 124.1, 125.0, and 123.6 mAh/g, respectively. When lithium excess amount increases from 0 to 6%, the discharge capacity is gradually increased because the excess Li^+ ions can occupy the vacant tetrahedral 8a site caused by the lithium loss during calcination process, thus resulting in more active Li^+ ions in the crystal lattice, which can be available in the charge/discharge process. However, when lithium excess amount is increased to 10%, the superfluous Li^+ ions are forced to occupy the octahedral 16d sites, which are electrochemically inactive, thus leading to the decrease of discharge capacity of LNMO-10% in comparison with LNMO-6%. In addition, the lowest impurity phase amount in LNMO-6% sample also accounts for its highest discharge capacity at low rate of 0.2 C.

Rate capability of $\text{LiNi}_{0.5}\text{Mn}_{1.5}\text{O}_4$ samples with different lithium excess amounts is depicted in Fig. 5b. The cells were charged and discharged at gradually elevated rates between 3.5 and 4.95 V. It can be seen that all samples show a decreasing discharge capacity with increasing current density, due to the increased ohmic and electrode polarization, which can also be seen from the growing voltage gap between charge and discharge curves in Fig. 5a. This decreased trend is amplified at higher rates of 5 and 10 C. As Fig. 5b demonstrates, LNMO-6% sample exhibits the best rate performance, whose discharge capacities are 125.0, 126.1, 124.2, and 118.9 mAh/g at 0.2-, 1-, 5-, and 10-C rates, respectively. The discharge capacity at 10-C rate accounts for 95.12% of that at 0.2-C rate, higher than 81.56% of LNMO-0, 87.11% of LNMO-2%, and 90.78% of LNMO-10%. This can be ascribed to the following reasons. Firstly, the higher Mn^{3+} content and disordering degree can enhance Li^+ ion transportation as well as electronic conductivity. Secondly, the larger lattice parameter is conducive to the Li^+ -ion diffusion in the material bulk.

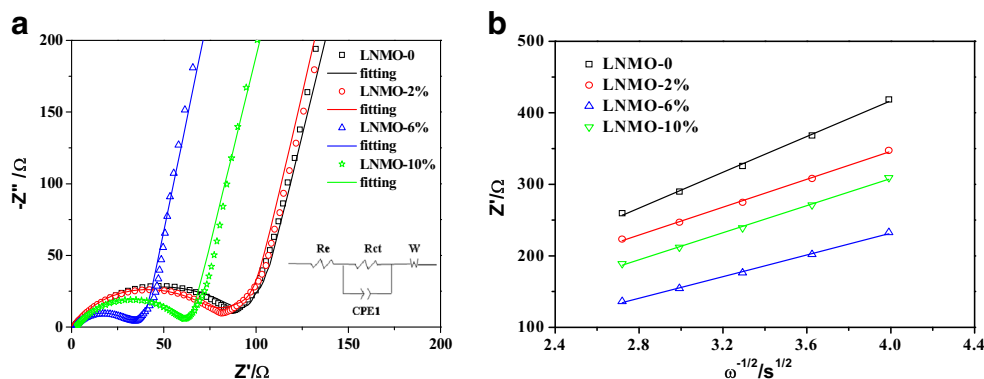
Thirdly, the lower cation mixing extent is also favorable to the Li^+ -ion diffusion and reduces the electrochemically inactive Li^+ ions at octahedral 16d site. It has been reported that the Li^+ -ion diffusion channel, 8a-16c-8a, is liable to be blocked by transition metal ions in tetrahedral 8a sites, therefore, avoiding the transition metal ion occupation in 8a sites is beneficial to Li^+ mobility [13]. The last one is the existence of less impurity phase. It is reported that the $\text{Li}_x\text{Ni}_{1-x}\text{O}$ impurity can lower the capacity and block Li^+ mobility in the material [14], which is bad for rate capability. Table S2 summarizes the rate performance of previously reported $\text{LiNi}_{0.5}\text{Mn}_{1.5}\text{O}_4$ sample synthesized via solid-state method. From these data, we can see that the rate performance of LNMO-6% sample exhibits higher discharge capacity at high rate, especially at 10-C rate.

Figure 6 shows the cycling performance curves of $\text{LiNi}_{0.5}\text{Mn}_{1.5}\text{O}_4$ samples with different lithium excess amounts at 1-C rate and room temperature. The increase of discharge capacity in the initial several cycles is called the activation process of the electrode due to the gradual infiltration of electrolyte into the inner part of the electrode. The 10th-cycle and 100th-cycle discharge capacities are used to calculate the capacity retention rates, which are 82.45, 89.24, 96.49 and 85.26% for LNMO-0, LNMO-2%, LNMO-6%, and LNMO-10%, respectively, suggesting that the LNMO-6% sample shows the best cycling performance. This can be attributed to higher Mn^{3+} content, higher phase purity, and lower cation mixing extent.

Table 2 Values of the CV peaks of $\text{LiNi}_{0.5}\text{Mn}_{1.5}\text{O}_4$ samples with different lithium excess amounts

Sample		φ_a (V)	φ_c (V)	$\Delta\varphi$ (mV)
LNMO-0	$\text{Ni}^{2+}/\text{Ni}^{3+}$	4.7484	4.6092	139.2
	$\text{Ni}^{3+}/\text{Ni}^{4+}$	4.8119	4.6557	156.2
LNMO-2%	$\text{Ni}^{2+}/\text{Ni}^{3+}$	4.7415	4.6195	122.0
	$\text{Ni}^{3+}/\text{Ni}^{4+}$	4.7950	4.6520	143.0
LNMO-6%	$\text{Ni}^{2+}/\text{Ni}^{3+}$	4.7359	4.6166	119.3
	$\text{Ni}^{3+}/\text{Ni}^{4+}$	4.7938	4.6565	137.3
LNMO-10%	$\text{Ni}^{2+}/\text{Ni}^{3+}$	4.7393	4.6047	134.6
	$\text{Ni}^{3+}/\text{Ni}^{4+}$	4.7991	4.6452	153.9

Fig. 8 Nyquist plots (a) and graphs of Z' plotted against $\omega^{-1/2}$ (b) of $\text{LiNi}_{0.5}\text{Mn}_{1.5}\text{O}_4$ samples with different lithium excess amounts



However, the LNMO-10% sample with lithium excess amount of 10% exhibits relatively worse cycling stability due to the heavier cation mixing and the existence of more $\text{Li}_x\text{Ni}_{1-x}\text{O}$ impurity phase, which is believed to be disadvantageous to structural stability. Due to the different test conditions, there is no comparability between the cycling performance data listed in Table S2 with that in the present work. But the $\text{LiNi}_{0.5}\text{Mn}_{1.5}\text{O}_4$ sample synthesized by a facile solid-state method with lithium excess amount of 6% exhibits satisfactory cycling performance on the whole.

Figure 7a shows the CV curves of $\text{LiNi}_{0.5}\text{Mn}_{1.5}\text{O}_4$ samples with different lithium excess amounts. From Fig. 7a, it can be seen that the split anodic peaks around 4.7 V and the existence of redox peaks around 4.0 V indicate that all four samples are mainly with disordered spinel phase. Table 2 lists the potential differences between the redox peaks of $\text{Ni}^{2+}/\text{Ni}^{3+}$ and $\text{Ni}^{3+}/\text{Ni}^{4+}$ reaction couples, which are 139.2/156.2 mV, 122.0/143.0 mV, 119.3/137.3 mV, and 134.6/153.9 mV for LNMO-0, LNMO-2%, LNMO-6%, and LNMO-10%, respectively, that is, the sample LNMO-6% shows the lowest potential difference, manifesting its lowest polarization degree and best reversibility, which leads to its optimum electrochemical performance. On the other hand, the peak area at ~ 4.0 V is related to Mn^{3+} content in spinel [26]. From the magnified image in Fig. 7b, it can be seen that the peak area, that is, Mn^{3+} content, first increases and then decreases with the lithium excess amount, which is in consistence with the above analysis results.

To better understand the effect of lithium excess amount on the electrochemical properties, electrochemical impedance spectroscopy (EIS) was carried out on the half-cell at fully discharged state after 3 cycles. Figure 8a presents the Nyquist plots of $\text{LiNi}_{0.5}\text{Mn}_{1.5}\text{O}_4$ samples with different lithium excess amounts from 100 kHz to 10 mHz. From Fig. 8a, we can see that all Nyquist plots are composed of a semicircle in the high-frequency region and a sloping line in the low-frequency region. The intercept of the semicircle at high frequency with the real axis refers to the ohmic resistance (R_e), and the diameter of this semicircle represents the charge transfer resistance (R_{ct}). The sloping line at low frequency is the

Warburg impedance (W), which is directly related to the Li^+ ion diffusion process in the electrode. Based on the ZView refinement results, we can get the charge transfer resistance values, which are 85.19, 71.65, 27.87, and 61.88 Ω for LNMO-0, LNMO-2%, LNMO-6%, and LNMO-10%, respectively. It can be concluded that the charge transfer resistance is first decreased and then increased with lithium excess amount increasing. Figure 8b shows the profiles of Z' vs. $\omega^{-1/2}$ in the low-frequency region. From the linear data fit of Z' vs. $\omega^{-1/2}$, the Warburg factor σ can be obtained. Putting the value of σ into the equation of $D_{\text{Li}} = 0.5R^2T^2/n^4A^2F^4C^2\sigma^2$ [27–29], the diffusion coefficients of Li^+ ions can be calculated, which are 2.13×10^{-11} , 9.22×10^{-11} , 1.27×10^{-10} , and 5.81×10^{-11} cm^2/s for LNMO-0, LNMO-2%, LNMO-6%, and LNMO-10%, respectively. From the above analysis, it can be concluded that the LNMO-6% sample shows the lowest charge transfer resistance and highest Li^+ -ion diffusion coefficient, which is believed to improve the electrochemical performance. It suggests that appropriate lithium excess amount can effectively improve the electrochemical kinetics of the electrode, thus leading to better rate capability and cycling performance, in accordance with the above electrochemical test results.

Conclusions

Spinel $\text{LiNi}_{0.5}\text{Mn}_{1.5}\text{O}_4$ cathode materials were synthesized via a facile solid-state method and the effects of different lithium excess amounts on the crystalline structure, particle morphology, and electrochemical performance were systematically investigated. SEM observation illustrates that the lithium excess amount has little influence on the particle morphology and size, whose significance on electrochemical performance can be excluded. XRD results show that with lithium excess amount increasing, the $\text{Li}_x\text{Ni}_{1-x}\text{O}$ impurity content and cation mixing extent first decrease and then increase, while the Mn^{3+} content (disordering degree) first increases and then decreases. The LNMO-6% sample with the highest phase purity and disordering degree exhibits the optimum electrochemical

performance, with discharge capacities of 125.0, 126.1, 124.2, and 118.9 mAh/g at 0.2-, 1-, 5-, and 10-C rates and capacity retention rate of 96.49% after 100 cycles at 1-C rate, which can be attributed to the lowest cation mixing extent, highest disordering degree, and phase purity. The slightly inferior electrochemical performance of LNMO-10% sample can be ascribed to the higher cation mixing extent and more $\text{Li}_x\text{Ni}_{1-x}\text{O}$ impurity phase. It can be concluded that in solid-state method, the lithium excess amount has little influence on particle morphology and size, and the electrochemical performance is mainly dependent on the crystalline structure, more specifically, Mn^{3+} content (disordering degree), $\text{Li}_x\text{Ni}_{1-x}\text{O}$ impurity amount (phase purity), and cation mixing extent.

Acknowledgements The authors are grateful to the Natural Science Foundation of Hebei Province (Grant number E2015202356), Key R&D Plan Self-raised Project of Hebei Province (Grant number 16214406), and Technology Innovation Foundation Project for Outstanding Youth of Hebei University of Technology (Grant number 2013009) for the financial support of this work.

References

- Zuo X, Zhu J, Müller-Buschbaum P, Cheng Y-J (2017) Silicon based lithium-ion battery anodes: a chronicle perspective review. *Nano Energy* 31:113–143. <https://doi.org/10.1016/j.nanoen.2016.11.013>
- Su D, Zhao Y, Yan D, Ding C, Ning M, Zhang J, Li J, Jin H (2017) Enhanced composite of V_2O_5 nanowires decorating on graphene layers as ideal cathode materials for lithium-ion batteries. *J Alloys Compd* 695:2974–2980. <https://doi.org/10.1016/j.jallcom.2016.11.363>
- Chen GH, Yang J, Tang JJ, Zhou XY (2015) Hierarchical NiCo_2O_4 nanowire arrays on Ni foam as an anode for lithium-ion batteries. *RSC Adv* 5(29):23067–23072. <https://doi.org/10.1039/C5RA00768B>
- Yang XL, Xing JL, Liu X, Wang T, Peng W, Xie J (2014) Performance improvement and failure mechanism of $\text{LiNi}_{0.5}\text{Mn}_{1.5}\text{O}_4$ /graphite cells with biphenyl additive. *Phys Chem Chem Phys* 16:24373–24381. <https://doi.org/10.1039/C4CP03173C>
- Xu Y, Wan L, Liu J, Zeng L, Yang Z (2017) γ -butyrolactone and glutaronitrile as 5 V electrolyte additive and its electrochemical performance for $\text{LiNi}_{0.5}\text{Mn}_{1.5}\text{O}_4$. *J Alloys Compd* 698:207–214. <https://doi.org/10.1016/j.jallcom.2016.11.381>
- Haridasa AK, Sharma CS, Rao TN (2016) Caterpillar-like sub-micron $\text{LiNi}_{0.5}\text{Mn}_{1.5}\text{O}_4$ structures with site disorder and excess Mn^{3+} as high performance cathode material for lithium ion batteries. *Electrochim Acta* 212:500–509. <https://doi.org/10.1016/j.electacta.2016.07.039>
- Yi T-F, Mei J, Zhu Y-R (2016) Key strategies for enhancing the cycling stability and rate capacity of $\text{LiNi}_{0.5}\text{Mn}_{1.5}\text{O}_4$ as high-voltage cathode materials for high power lithium-ion batteries. *J Power Sources* 316: 85–105. <https://doi.org/10.1016/j.jpowsour.2016.03.070>
- Gu Y-J, Li Y, Chen Y-B, Liu H-Q (2016) Comparison of Li/Ni antisite defects in $\text{Fd}3m$ and $\text{P}4_332$ nanostructured $\text{LiNi}_{0.5}\text{Mn}_{1.5}\text{O}_4$ electrode for Li-ion batteries. *Electrochim Acta* 213:368–374. <https://doi.org/10.1016/j.electacta.2016.06.124>
- Kim JH, Pieczonka NPW, Li Z, Wu Y, Harris S, Powell BR (2013) Understanding the capacity fading mechanism in $\text{LiNi}_{0.5}\text{Mn}_{1.5}\text{O}_4$ /graphite Li-ion batteries. *Electrochim Acta* 90:556–562. <https://doi.org/10.1016/j.electacta.2012.12.069>
- Liu J, Manthiram A (2009) Understanding the improved electrochemical performances of Fe-substituted 5 V spinel cathode $\text{LiMn}_{1.5}\text{Ni}_{0.5}\text{O}_4$. *J Phys Chem C* 113(33):15073–15079. <https://doi.org/10.1021/jp904276t>
- Chemelewski KR, Manthiram A (2013) Origin of site disorder and oxygen nonstoichiometry in $\text{LiMn}_{1.5}\text{Ni}_{0.5-x}\text{M}_x\text{O}_4$ ($\text{M}=\text{Cu}$ and Zn) cathodes with divalent dopant ions. *J Phys Chem C* 117(24):12465–12471. <https://doi.org/10.1021/jp404496j>
- Qian Y, Deng Y, Wan L, Xu H, Qin X, Chen G (2014) Investigation of the effect of extra lithium addition and post-annealing on the electrochemical performance of high-voltage spinel $\text{LiNi}_{0.5}\text{Mn}_{1.5}\text{O}_4$ cathode material. *J Phys Chem C* 118(29):15581–15589. <https://doi.org/10.1021/jp503584k>
- Deng Y-F, Zhao S-X, Zhai P-Y, Cao G, Nan C-W (2015) Impact of lithium excess on the structural and electrochemical properties of $\text{LiNi}_{0.5}\text{Mn}_{1.5}\text{O}_4$ high-voltage cathode material. *J Mater Chem A* 3(40):20103–20107. <https://doi.org/10.1039/C5TA06339F>
- Xue Y, Wang Z, Zheng L, Yu F, Liu B, Zhang Y, Ke K (2015) Investigation on preparation and performance of spinel $\text{LiNi}_{0.5}\text{Mn}_{1.5}\text{O}_4$ with different microstructures for lithium-ion batteries. *Sci Rep* 5(1):13299. <https://doi.org/10.1038/srep13299>
- Feng J, Huang Z, Guo C, Chernova NA, Upreti S, Whittingham MS (2013) An organic coprecipitation route to synthesize high voltage $\text{LiNi}_{0.5}\text{Mn}_{1.5}\text{O}_4$. *ACS Appl Mater Interfaces* 5(20):10227–10232. <https://doi.org/10.1021/am4029526>
- Thackeray MM (1997) Manganese oxides for lithium batteries. *Prog Solid State Chem* 25(1-2):1–71. [https://doi.org/10.1016/S0079-6786\(97\)81003-5](https://doi.org/10.1016/S0079-6786(97)81003-5)
- Bao SJ, Li CM, Li HL, Luong JHT (2007) Morphology and electrochemistry of LiMn_2O_4 optimized by using different Mn-sources. *J Power Sources* 164(2):885–889. <https://doi.org/10.1016/j.jpowsour.2006.11.015>
- Wei YJ, Nam KW, Kim KB, Chen G (2006) Spectroscopic studies of the structural properties of Ni substituted spinel LiMn_2O_4 . *Solid State Ionics* 177(1-2):29–35. <https://doi.org/10.1016/j.ssi.2005.10.015>
- Lee YS, Kumada N, Yoshio M (2001) Synthesis and characterization of lithium aluminum-doped spinel ($\text{LiAl}_x\text{Mn}_{2-x}\text{O}_4$) for lithium secondary battery. *J Power Sources* 96(2):376–384. [https://doi.org/10.1016/S0378-7753\(00\)00652-2](https://doi.org/10.1016/S0378-7753(00)00652-2)
- Yi T-F, Han X, Chen B, Zhu Y-R, Xie Y (2017) Porous sphere-like $\text{LiNi}_{0.5}\text{Mn}_{1.5}\text{O}_4$ - CeO_2 composite with high cycling stability as cathode material for lithium-ion battery. *J Alloys Compd* 703: 103–113. <https://doi.org/10.1016/j.jallcom.2017.01.342>
- Ariyoshi K, Iwakoshi Y, Nakayama N, Ohzuku T (2004) Topotactic two-phase reactions of $\text{Li}[\text{Ni}_{1/2}\text{Mn}_{3/2}]\text{O}_4$ ($\text{P}4_332$) in nonaqueous lithium cells. *J Electrochem Soc* 151(2):A296–A303. <https://doi.org/10.1149/1.1639162>
- Kunduraci M, Amatucci GG (2008) The effect of particle size and morphology on the rate capability of 4.7 V $\text{LiMn}_{1.5+x}\text{Ni}_{0.5-x}\text{O}_4$ spinel lithium-ion battery cathodes. *Electrochim Acta* 53(12): 4193–4199. <https://doi.org/10.1016/j.electacta.2007.12.057>
- Lee E-S, Manthiram A (2013) Influence of doping on the cation ordering and charge-discharge behavior of $\text{LiMn}_{1.5}\text{Ni}_{0.5-x}\text{Mn}_x\text{O}_4$ ($\text{M}=\text{Cr}$, Fe , Co , and Ga) spinels between 5.0 and 2.0 V. *J Mater Chem A* 1(9):3118–3126. <https://doi.org/10.1039/c2ta01171a>
- Lee E-S, Nam K-W, Hu E, Manthiram A (2012) Influence of cation ordering and lattice distortion on the charge-discharge behavior of $\text{LiMn}_{1.5}\text{Ni}_{0.5}\text{O}_4$ spinel between 5.0 and 2.0 V. *Chem Mater* 24(18): 3610–3620. <https://doi.org/10.1021/cm3020836>
- Zeng Y-P, Wu X, Mei P, Cong L-N, Yao C, Wang R-S, Xie H-M, Sun L-Q (2014) Effect of cationic and anionic substitution on the electrochemical properties of $\text{LiNi}_{0.5}\text{Mn}_{1.5}\text{O}_4$ spinel cathode materials. *Electrochim Acta* 138:493–500. <https://doi.org/10.1016/j.electacta.2014.06.082>
- Hai B, Shukla AK, Duncan H, Chen G (2013) The effect of particle surface facets on the kinetic properties of $\text{LiMn}_{1.5}\text{Ni}_{0.5}\text{O}_4$ cathode

- materials. *J Mater Chem A* 1(3):759–769. <https://doi.org/10.1039/C2TA00212D>
27. Luo D, Li G, Yu C, Yang L, Zheng J, Guan X, Li L (2012) Low-concentration donor-doped LiCoO_2 as a high performance cathode material for Li-ion batteries to operate between -10.4 and 45.4 °C. *J Mater Chem* 22(41):22233–22241. <https://doi.org/10.1039/c2jm35550g>
28. Xiang JY, JP T, Qiao YQ, Wang XL, Zhong J, Zhang D, CD G (2011) Electrochemical impedance analysis of a hierarchical CuO electrode composed of self-assembled nanoplates. *J Phys Chem C* 115(5):2505–2513. <https://doi.org/10.1021/jp108261t>
29. Li B, Han C, He Y-B, Yang C, Du H, Yang Q-H, Kang F (2012) Facile synthesis of $\text{Li}_4\text{Ti}_5\text{O}_{12}/\text{C}$ composite with super rate performance. *Energy Environ Sci* 5(11):9595–9602. <https://doi.org/10.1039/c2ee22591c>